Cent. Eur. J. Geosci. • 2(3) • 2010 • 399-419
DOI: 10.2478/v10085-010-0015-6

VERSITA

Central European Journal of **Geosciences**

Volcanic glass textures, shape characteristics and compositions of phreatomagmatic rock units from the Western Hungarian monogenetic volcanic fields and their implications for magma fragmentation

Research Article

Károly Németh*

Volcanic Risk Solutions CS-INR, Massey University, Palmerston North, New Zealand

Received 2 April 2010; accepted 17 May 2010

Abstract: The majority of the Mio-Pleistocene monogenetic volcanoes in Western Hungary had, at least in their initial eruptive phase, phreatomagmatic eruptions that produced pyroclastic deposits rich in volcanic glass shards. Electron microprobe studies on fresh samples of volcanic glass from the pyroclastic deposits revealed a primarily tephritic composition. A shape analysis of the volcanic glass shards indicated that the fine-ash fractions of the phreatomagmatic material fragmented in a brittle fashion. In general, the glass shards are blocky in shape, low in vesicularity, and have a low-to-moderate microlite content. The glass-shape analysis was supplemented by fractal dimension calculations of the glassy pyroclasts. The fractal dimensions of the glass shards range from 1.06802 to 1.50088, with an average value of 1.237072876, based on fractal dimension tests of 157 individual glass shards. The average and mean fractal-dimension values are similar to the theoretical Koch-flake (snowflake) value of 1.262, suggesting that the majority of the glass shards are bulky with complex boundaries. Light-microscopy and backscattered-electron-microscopy images confirm that the glass shards are typically bulky with fractured and complex particle outlines and low vesicularity; features that are observed in glass shards generated in either a laboratory setting or naturally through the interaction of hot melt and external water. Textural features identified in fine- and coarse-ash particles suggest that they were formed by brittle fragmentation both at the hot melt-water interface (forming active particles) as well as in the vicinity of the interaction interface. Brittle fragmentation may have occurred when hot melt rapidly penetrated abundant water-rich zones causing the melt to cool rapidly and rupture explosively.

Keywords: volcanic glass • fractal • shape • fragmentation • sideromelane • MFCI

1. Introduction

Volcanic glass shards are chilled fragments of magma that represent rapid cooling of the melt upon fragmentation [1]. Volcanic glass shards are commonly formed during phreatomagmatic explosions where rising magma interacts

*E-mail: k.nemeth@massey.ac.nz

with external water [2]. The shape, crystallinity, vesicularity and surface texture of the volcanic glass shards reflect the complex processes that occur when hot melt interacts with cold external water [3, 4].

Brittle-melt fragmentation coupled with the release of relatively high amounts of kinetic energy result in the production of fine-ash fragments during thermohydraulic explosions [4, 5]. Therefore, the shape and texture of fine-ash particles (<2 Φ) formed during explosive fragmentation can be used to examine the processes that occur during the thermal-to-kinetic energy transition [2, 3, 6–9]. These particles are commonly referred to as active particles because of the active role they play in the thermal-to-kinetic energy transfer during phreatomagmatic explosions [3, 10–13]. While the phreatomagmatic fragmentation (e.g. brittle-melt fragmentation) quickly vaporizes the adjacent water, the sudden vapour expansion deforms the melt immediately surrounding the explosion locus triggering ductile deformation and the consequent spallation of the particles into the expanding pyroclastic mixture [3, 4, 13]. Textural features of pyroclasts, such as shape parameters that are indicative of either brittle-melt deformation or ductile-melt deformation, provide information about the melt fragmentation history [4]. Accordingly, pyroclast morphologies and textural characteristics from a statistically-significant amount of pyroclasts from stratigraphically controlled pyroclastic successions that are phreatomagmatic in origin can provide very detailed information on the brief shifts (hours-to-days) in magma fragmentation styles [14–23] that commonly occurs during monogenetic eruptions. Therefore, accurate descriptions of the pyroclasts' geometrical parameters can be used to determine the style of magma/water interaction and the events that follow prior to eruption [4].

Textural studies of volcanic glass date back to the early 1980s. Since then there have been significant advances in the understanding of how glassy pyroclasts form and the methods used to quantitatively and qualitatively describe and discriminate between shapes and textures of various pyroclasts [15, 24–26]. Recent studies involving geometrical-shape analysis methods examined primarily young and fresh pyroclasts [15, 26–28]. Such material easily disaggregates allowing for individual ash particles to be picked and analyzed independently using 3D scanning electron microscopy (SEM) methods [9]. The analysis of 2D particle images involves the use of particle-shape descriptors [13, 15, 28–34]. While numerous studies have utilized data derived from individual ash particles, few have attempted to apply this method to lithified pyroclastic rocks. This paper records the first attempt to characterise the ash particle geometry of lithified phreatomagmatic pyroclastic rocks preserved from a Mio-Pleistocene monogenetic volcanic field in Western Hungary.

2. Phreatomagmatic Volcanic Fields

Phreatomagmatic volcanic fields in continental settings [21] are repeatedly the focus of studies examining pyroclastic texture and structure because of their frequent occurrence in a variety of geotectonic settings worldwide, often in heavily populated areas such as the Auckland volcanic field in New Zealand [35, 36]. It is important, particularly from a volcanic hazard perspective, to understand the last stage of magma fragmentation immediately preceding eruption. This information is crucial to accurately characterize the volcanic hazard potential that an explosive eruption triggered by magma-water interaction poses to the surrounding environment.

Maar volcanoes that form due to the explosive interaction of rising magma and various types of ground-water sources are especially valuable to textural and morphological analyses of volcanic glass as these studies provide insight into the energy-transfer process involved as magma undergoes rapid cooling during phreatomagmatic eruptions. This process provides enough kinetic energy to trigger melt fragmentation and transport the resulting pyroclasts to the depositional sites via eruption eventually leading to a mass deficit and structural collapse, forming a maar. It is also vital to be able to distinguish between active and non-active pyroclasts preserved in pyroclastic deposits. The total volume of fine-ash particles with geometrical parameters associated with brittle transformation (e.g. active particles) can be used to estimate the explosivity of the eruption because they were formed as a result of the transfer of thermal energy to kinetic energy (e.g. the force responsible for driving particles away from the explosion locus) [2, 3].

Glassy pyroclasts are not only abundant in maar-forming tephra-ring beds, but also accumulate in diatremes [37, 38]. In older phreatomagmatic volcanic terrains, the diatreme may be the only part of a maar-diatreme volcano that is preserved [39–43]. Therefore, any textural information about the volcanic glass derived from a maar-diatreme volcano can advance the current understanding of the fragmentation process that drove the entire eruption. Although glassy pyroclasts are a common occurrence in diatreme-filling pyroclastic rock units, it is likely that their textural characteristics will reflect a diverse and complex fragmentation history that was strongly influenced by the conduit dynamics of the growing maar volcano [37, 41, 44]. While pyroclastic rocks formed in diatremes are not ideal subjects for this type of analysis, they are often the only

rocks preserved in older volcanic fields, and therefore, the only samples available to examine the style and process involved in their creation.

3. Geological Setting

The Carpathian-Pannonian Region (CPR) contains a wide range of volcanic rocks formed during the last 20 Ma (Figure 1). The volcanic rocks are associated with the combined processes of large-scale block translation, subduction and extension [45, 46]. The subduction of oceanic lithosphere occurred along the curvilinear belt of the present Outer-Carpathians [46]. Subduction gradually halted from the west to east-southeast during the Middle Miocene to Pliocene [46]. Behind the subduction zone in the back arc, the Pannonian Basin (Figure 1) was formed by lithospheric extension [47]. During the Palaeogene–Early Miocene period, the rate of convergence was greater than the rate of subduction causing the upper plate to regionally deform via horizontal shortening [48, 49]. A significant change in subduction style during the Late Miocene triggered a shift in the deformational character of the overriding plate from a compressional regime to an extensional setting [49]. As the subduction style varied from advancing to retreating, the slab cooled causing it to sink rapidly, leading to lithospheric stretching in the back-arc region [49–52]. This period is known as the active rift phase (intense extension, subsidence and voluminous volcanism) in the evolution of the Pannonian Basin (Early to Middle Miocene), and was followed by the post rift phase in the Late Miocene (~11 Ma) [49]. During the post rift phase, small-volume mostly alkaline basaltic volcanic fields formed unsystematically in well-distinguished zones in the Pannonian Basin [46, 49, 53, 54].

In the western part of the Pannonian Basin (mostly in Hungary), partial melting in the asthenospheric mantle formed two distinct volcanic fields (Figure 1) composed of mainly of alkali olivine basalt and basanites with a relict subduction signature [47, 55, 56].

The larger and more centrally located field, the Bakony-Balaton Highland Volcanic Field (BBHVF) (Figure 1), represents a long lived, low volume, typical intra-plate volcanic field with a variety of eruption styles [57]. Activity started in the east (Tihany peninsula) around 8 Ma years ago [58]; a date consistent with recently dated, strongly eroded diatreme remnants [59, 60]. The youngest volcanoes occurred in the western part of the field about 2.3 Ma years ago [54, 60]. Many volcanoes in the central part of the field developed between 3 and 5 Ma, marking the culmination of eruptive activity [60]. From a morphological point of view, the BBHVF is characterized by erosional remnants of maars, tuff rings, scoria cones, and shield volcanoes [61]. Pyroclastic density current deposits were preserved inside the craters, volcanic conduits or proximal to the crater rim and are the only remaining volcanic rocks [43]. The geographical distribution of different vent types seems to relate to the general hydrogeological characteristics of the pre-volcanic rock units and the surface water distribution and fracture network of the deeper, hard rocks [43].

The other distinct volcanic field that is similar in age to the BBHVF is located just to the NW of the BBHVF and is referred to as the Little Hungarian Plain Volcanic Field (LHPVF) (Figure 1) [43]. The magma composition and eruptive styles that formed the preserved volcanic rocks in this field are similar to those recognized at the BBHVF. However, the preserved volcanic edifices seem to represent far broader volcanic landforms dominated by broad and flat tuff rings commonly filled with small-volume magmatic explosive and or effusive products [62]. Similarly, the vent distribution pattern of the LHPVF is more likely related to the known deep fault system running NE-SW through the field [43]. The LHPVF also has far fewer (at least 7 while the BBHVF has around 50) and less closely spaced vents than the BBHVF with eruptions slightly predating the peak activity at the BBHVF at around 5 Ma [43].

The country rock characteristics also differ between the BBHVF and LHPVF. While the BBHVF's basement comprises mostly Silurian schist, Permian red sandstone, and Mesozoic carbonates (mainly dolomite and limestone), the basement of the LHPVF is mostly crystalline rocks [43]. In addition to these differences, the basement rocks at the BBHVF are located near surface, while at the LHPVF they underlie thousands of metres of Neogene siliciclastic successions. The younger, adjacent pre-volcanic successions in both fields consist of complex Tertiary sediment of Paratethys (e.g. sand, gravel, marl, clay, limestone and silt) [63].

Prior to volcanism, the successor of the Paratethys large lake system, Lake Pannon, formed. This lake was gradually filled in by sediment input from large river networks to the north. About 9–8 Ma Lake Pannon devolved from the present day region of the LHPVF and BBHVF [63, 64].

The deposits comprising the Paratethys system, and subsequent Lake Pannon, are still unconsolidated today, and were likely saturated with water during the time of volcanism, providing a good aquifer to feed explosive magma-water interactions [43]. The BBHVF erosional remnants of monogenetic volcanoes are distributed in a slightly N–S and NE–SW alignment inferred to reflect the structurally controlled network of fluvial channels that were most likely the site of phreatomagmatic eruptions [43]. In the case of the BBHVF, it has been surmised that not only the up-

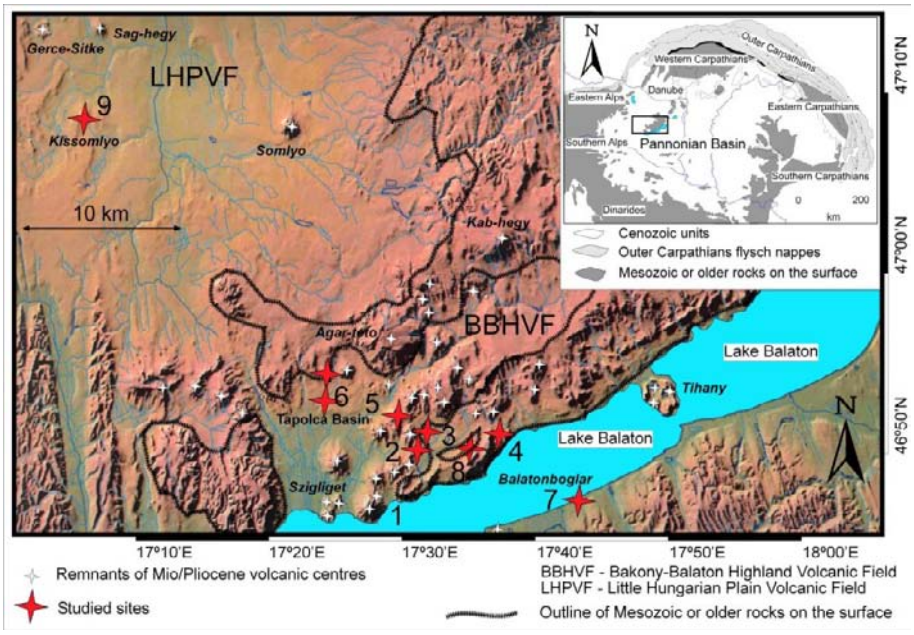

Figure 1. Overview map of the Mio-Pleistocene monogenetic volcanic fields in western Hungary. Numbers represent those sites from where volcanic glass shape and fractal dimension studies were carried out; 1 – Hármas-hegy diatreme (H3-1), 2 – Kékkút diatreme (D1), 3 – Kereki-domb diatreme (K1), 4 – Zánkai Vár-hegy diatreme (ZV), 5 – Hajagos maar-tuff ring (H2), 6 – Véndek-hegy diatreme (V1), 7 – Boglár diatreme (BOG), 8 – Kis-hegyestű diatreme (KH), 9 – Kissomlyó maar-tuff ring (KS)

permost Neogene siliciclastic units, but also the Mesozoic carbonate rocks and the deeper "hard rocks", must have functioned as "fracture-controlled" aquifers, providing excellent water sources to fuel phreatomagmatism [65, 66]. These spatial distribution patterns suggest that the style of phreatomagmatism and resulting volcanic landforms were strongly controlled by the type of country rock and its hydrogeology. The thick siliciclastic Neogene basin at the LHPVF provided ideal conditions for the formation of laterally growing broad tuff rings. In contrast, it is evident that the formation of phreatomagmatic volcanoes at the BBHVT was controlled by both a dual water source and also the structural character of the country.

4. Mio-Pleistocene Phreatomagmatic Pyroclastic Successions of Western Hungary

The most pervasive geomorphologic formations in the Mio-Pleistocene volcanic fields of Western Hungary are the circular, mostly lava capped, buttes. These centres are usually related to underlying maar structures and occasionally to eroded tuff-ring-rim remnants in areas where lava flows preserved them. Individual maar structures without lava infill are less common, and hard to identify in the field. They usually consist of the remains of late maar crater-lake filling sediments.

The water source for the explosive magma-water interaction-triggered eruption of the monogenetic volcanoes of Western Hungary was inferred to be ground water, as suggested from the abundance of country rocks (accidental lithic fragments) in most of the pyroclastic successions (Figure 2A, B). The eruptions produced maar-diatreme structures, which were later filled by maar lake volcaniclastics followed by fresh water carbonate beds and magmatic products including Strombolian scoria cones or lava flows.

The small (ash size), chilled, blocky sideromelane glassy shards (Figure 2C) with low vesicularity (Figure 2D) represent phreatomagmatic explosion products characteristic of deposits from Western Hungary. The juvenile particles coarser-than-fine ash are considered to be non-interactive (e.g. volcanic lithic fragments – Figure 2D) and are abundant in many pyroclastic rocks from Western Hungary.

Preserved pyroclastic rock units from the Western Hungarian Neogene volcanic fields are thought to have formed from highly expanded, turbulent, gravity-driven pyroclastic currents, such as base surges (Figure 2A). Pyroclastic rocks formed from base surges in Western Hungary are typically wavy and contain bed-forms, rim-type accretionary lapilli, ballistic impact sags, abundant volcanic

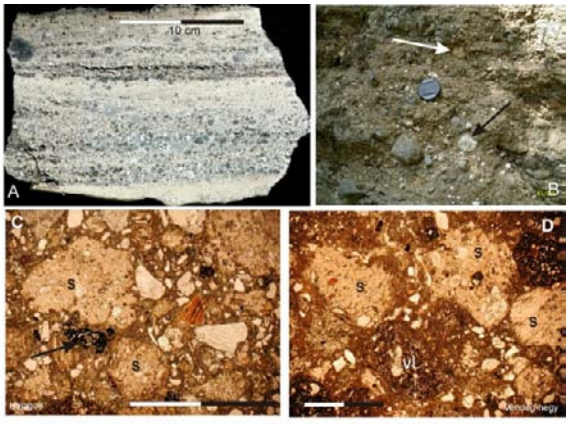

Figure 2. (A) Typical bedded lapilli tuff and tuff section from a basal phreatomagmatic unit of a proximal succession of an erosion remnant of a western Hungarian phreatomagmatic volcanio.
(B) Coarse grained, massive lapilli tuff of the Pula maar proximal crater rim facies. The lapilli tuff is rich in accidental lithic fragments such as sandstone from the Miocene silicilastic successions (white arrow) and limestones, dolomites from the Mesozoic carbonate successions (black arrow).
(C) Typical lapilli tuff in microphotograph from the Hajagos maar-tuff ring pyroclastic succession. Sideromelan (S) glass shards are moderately vesicular, blocky, and their boundary is bulbous. The lapilli tuff has also some tachylitic ash (black arrow).
(D) Typical lapilli tuff from the Vendek-hegy diatreme rich in sideromelane glass shards (S) with various but low vesicularity, blocky shape and sharp edges. The lapilli tuff contains some volcanic lithic fragments (vl).

and non-volcanic lithic fragments (Figure 2B), and show evidence of cohesion, suggesting a water surplus in the transportion current prior to deposition.

In Western Hungary the basal pyroclastic successions are, in nearly all volcanic relics, composed of alternating beds of base-surge and fall-out deposits Pyroclastic- density-current deposits that are more consistent with dryer surge activity seem to be more common in those areas where the preserved volcanic remnants are situated in thick, siliciclastic deposit-filled basins, such as in the Tapolca Basin in the western part of the BBHVF or in the LHPVF.

The volcanic remains of Western Hungary are exposed at the subsurface to surface levels, but are usually covered by Holocene talus deposits. The level of exposures at most of the known eruptive points indicate that the present day surface rocks represent exposed diatreme facies, a former sub-surface architecture of maar-diatreme volcanoes [57, 61, 67]. While a general trend cannot yet be discerned, it seems that the deepest exposures of diatreme facies are located in the southern and western part of the BBHVF, whereas the erosional vestiges of the LHPVF represent volcanic facies near the surface. The most strongly eroded regions in the BBHVF are those where no subsequent lava caps the volcaniclastic sequences, such as the Balatonboglár, Szigliget, Tihany Peninsula. In many cases, these sites contain coherent magmatic rocks, such as dykes that intruded into the host pyroclastic diatreme facies successions, commonly with irregular margins inferred to be peperites [68].

The matrix of the base-surge beds commonly contains a high proportion of sand from the pre-volcanic Neogene siliciclastic sediments (Figure 2C, D), especially in those areas where the adjacent pre-volcanic country rocks are Neogene siliciclastic sediments.

In this study an electron microprobe analysis of the glass shards was performed on fresh pyroclastic rocks from the majority of the known eruptive centres; locations are marked in Figure 1.

In order to accurately depict glass-shard morphology, samples were selected primarily from well-confined pyroclastic rock outcrops interpreted to be deeply eroded successions and exposures of diatreme facies from phreatomagmatic volcanoes. Samples included materials from phreatomagmatic diatreme-filling successions of the Hármas-hegy diatreme (H3-1), Véndek-hegy diatreme (V1), Kereki-domb diatreme (K1), Zánkai varhegy diatreme (ZV), Kis-hegyes-tű diatreme (KH), Kékkút diatreme (D1) and Boglár diatreme (BOG). The characteristics commonly observed in the pyroclastic rock sampled include 1) a massive, unsorted nature, 2) a geographically well-confined distribution, 3) being situated in an angular unconformity to the host country rocks, 4) common cross-cutting relationships with small dykes that are inferred to be feeder dykes, and 5) distinct lateral variation of grain size, bedding orientation and juvenile-to-accidental lithic ratio. The physical volcanology of these sites has been described in detail [69]. In addition to analyzing the glassy particles from phreatomagmatic rocks from the smallest preserved diatremes in the region, samples were also selected from two sites (Kissomlyó maar/tuff ring - KS and Hajagos maar/tuff ring – H2) including proximal base-surge beds that had accumulated in the phreatomagmatic crater. These samples were collected from inward dipping, unsorted, accidental lithic-rich, lapilli-tuff beds formed from base surges triggered by magma-and-water interaction.

5. Methodology

Extensive exposures of conduit filling and proximal phreatomagmatic successions found in vast quarry faces provided a great opportunity to collect samples of pyroclasts accumulated around vents in Western Hungary

for micro-morphology analyses. The goal of these micro-morphology studies was to characterize the particle shape, composition, and grain size distribution of juvenile pyroclasts in order to determine the potential magma fragmentation, pyroclast transportation, and deposition processes associated with phreatomagmatic explosive eruptions. Representative rock units were selected from various erosional remnants from known and well-established stratigraphic positions. In this study, we aimed to provide a first order approach to understanding the fragmentation history of individual vents without completing detailed stratigraphic sections at each site. In this way, our study is only representative of the general magma-fragmentation pattern of Western Hungarian Neogene intra-plate volcanism and cannot be used to understand the small-scale variation that an individual volcano may undergo during the course of otherwise short-lived explosive eruptions. This work is the first time a study has attempted to identify key textural features of the glassy pyroclasts of Western Hungary laying the groundwork for more detailed studies in the future, as well as documenting the first research effort evaluating the efficacy of detailed pyroclastic textural studies of relatively older phreatomagmatic volcanic fields.

All analytical work was performed on polished petrologic thin sections. Due to the strong diagenetic quality of the the majority of the pyroclastic rock units, accurate grain disaggregation was not possible without destroying the original shape of the pyroclasts. Therefore, textural information was achieved by using polished petrologic thin sections. Complications with this method included: 1) the pyroclasts' morphologies were derived from two dimensional images that represented only one slice of a real particle, and 2) the heterogeneous nature of the rock samples meant that the perimeters of the clasts were occasionally obscured by palagonitization and/or other surface processes, making image processing time consuming. One benefit of this method is that the relative ease involved in the creation of thin sections allowed for numerous sections to be created from a single rock sample, increasing the number of sections available for analysis and thereby increasing the data set.

Electron microprobe analysis was performed on individual glass particles to establish major element compositions. Juvenile particles were selected for backscattered electron microscopy (BSE) to determine their morphological parameters. The morphological analysis of the juvenile particles was aided by light microscopy (LM). The generated images were then analysed using image analysis methods to characterize the shape parameters of the juvenile particles in order to make interpretations about the the fragmentation mode indicated by each shape, following methods described by Büttner et al (2000) and references therein.

6. Volcanic Glass Composition

The electron microprobe study was performed on a JEOL 9600 hosted at the University of Otago using 20 kV acceleration voltage, 5 to 25 micron beam diameter and ZAF correction method to recalculate oxide values. The samples selected were fresh with no apparent or extensive alteration observed on the surface of the ash- to fine-lapilli sized particles. The totals of each measurement were around 96 wt% which is considered to be acceptable for basaltic glass compositions. The compositional values have been recalculated to volatile free 100% total values. Data were plotted using *Petrograph Freeware* (http://www.unipg.it/~maurip/SOFTWARE.htm) [70].
When possible, vesicle- and microlite-poor glassy pyroclasts were measured; however, the pyroclasts were often extensively fractured ash particles showing initial hydration along rims and fractures. In such cases, measurements were taken from fresh glass surfaces using small (5-15 micron) electron beam diameters to avoid "sampling" alteration and/or microlite content.

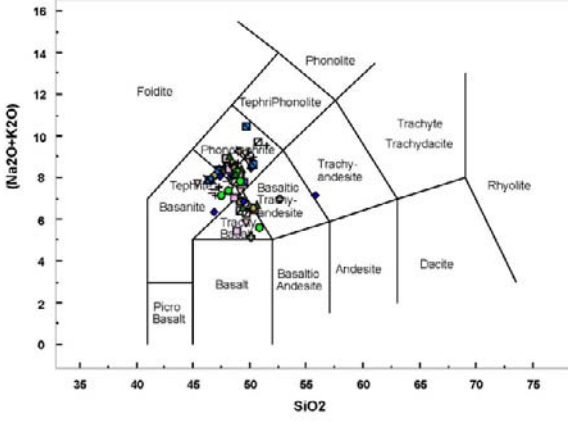

Figure 3. TAS-diagram of volcanic glass shards of phreatomagmatic pyroclastic successions of the western Hungarian Mio-Pleistocene monogenetic volcanic fields. Note the compositional variation centered around the tephritic, phono tephritic composition.

The major element composition revealed that the majority of the volcanic glass shards were tephritic to phonotephritic in composition (Figure 3). The total alkali content of the particles ranges between 5 and 12 wt%, indicating a moderate to strong alkaline compositional trend

(Figure 3). Harker diagrams of the glass shards plotted in a well confined field in each discrimination diagram (Figure 4); however, a trend indicative of crystal fractionation can be recognized in the overall data distribution patterns. In general, the variation among compositional data from individual eruptive points (Szigliget diatreme) was narrow (Figure 5), signifying the primarily monogenetic nature of the small-volume basaltic volcanoes, at least the phreatomagmatic eruptive phases. While the bulk composition of individual sites, like the aforementioned Szigliget diatreme, suggested a narrow compositional field (tephrite), data from the individual glass shard compositions from Szigliget plotted on Harker diagrams revealed clear trends, indicating some potential chemical variations (Figure 6). These trends need to be examined in detail in the future to determine how they may relate to temporal variations and potential changes in the texture of pyroclastic deposits from the otherwise small-volume volcanoes.

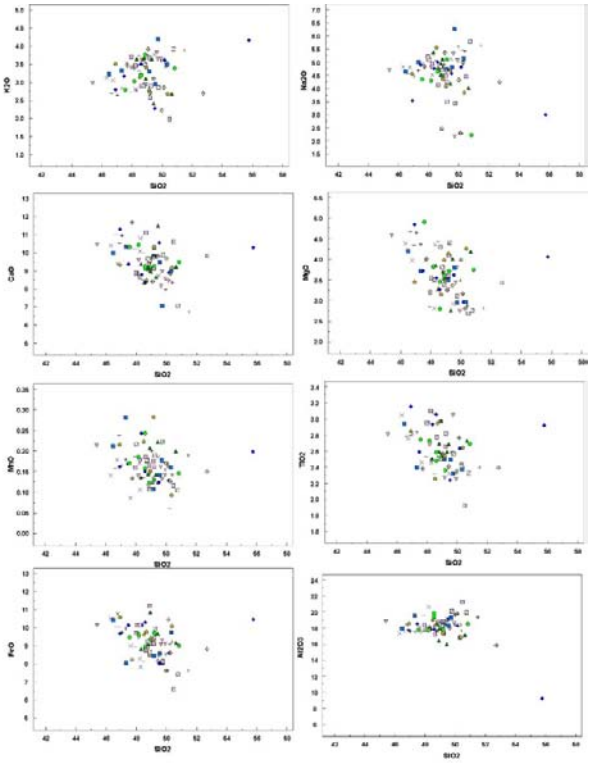

Figure 4. Harker-diagrams of the volcanic glass shards studied so far from the entire western Hungarian young monogenetic volcanic fields. The compositional range is narrow, however the values plotted along a lineament commonly suggesting crystal fractionation.

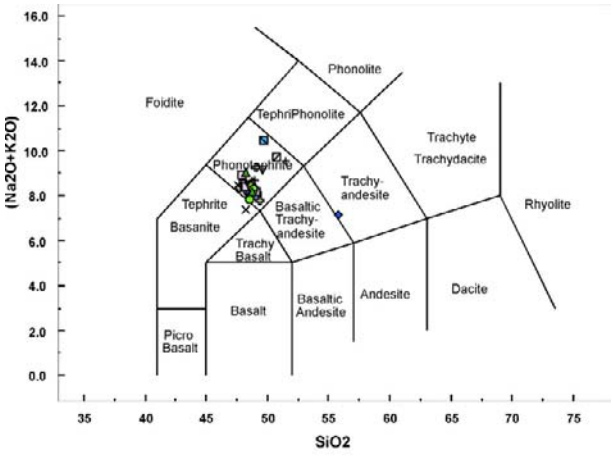

Figure 5. TAS-diagram of glass shard analysis from a single location (Szigliget diatreme) shows similar narrow compositional values as the overall analysis from the entire field.

7. Light Microscopy

Light microscopy was applied to each of the polished thin sections of the phreatomagmatic lapilli tuff samples (Figure 2C,D). The glassy pyroclasts were examined and their morphological and textural features described. Fine-ash sized glassy pyroclasts were looked at in more detail, with an aim to identify the textural characteristics of the potential interactive particles. In addition, light microscopy images were analyzed to describe the shape parameters of the juvenile particles. The light microscopy data derived from petrographic thin sections were not suitable for detailed particle shape analysis due to difficulties in generating black and white bitmap images of the highly varied colour images provided by the LM method.
Petrologic microscopy on the majority of the samples revealed at least 3 basic types of glassy pyroclast textures:

1. moderately-vesicular coarse ash/fine lapilli (Figure 2C),
2. microlite-bearing coarse ash/fine lapilli (Figure 2D),
3. non-vesicular fine ash. Coarse-ash to fine-lapilli sized glassy pyroclasts were generally complex in shape (Figure 2C,D).

Their vesicularity, calculated using vesicle surface area measurements of retraced glass shard and vesicle outlines, varied from nearly zero to about 30%, but the dominant vesicularity was low, about 10%. The vesicles were

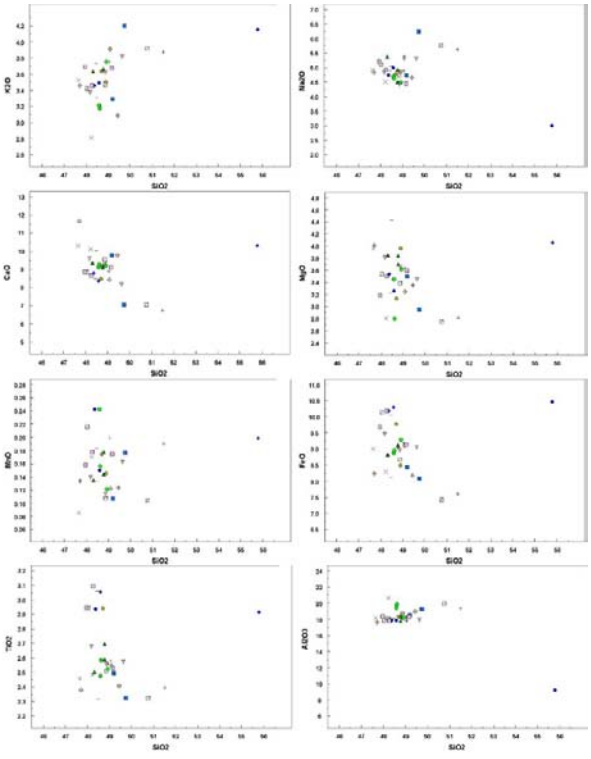

Figure 6. Harker-diagrams of glass shard compositional data from a single location (Szigliget diatreme) show similar trends as the overall data from the western Hungarian young monogenetic volcanic fields.

rarely interconnected, and their shapes ranged from symmetric to strongly flattened. Elongated vesicles were often aligned creating an overall fluidal texture within the glassy pyroclasts. Conversely, fine ash was almost exclusively non-vesicular, bulky, and angular in shape. Coarse ash and fine lapilli varied greatly in crystallinity; however, the majority of the larger glassy pyroclasts contained at least 10% (surface area) microlites and micro-crystals of plagioclase, pyroxene and olivine pyrogenic crystals.

The glassy particles were heavily fractured, regardless of their size, and contained micro-fracture networks. The micro-fractures often represent the initiation of palagonite formation. The edges of the coarser grained glassy particles are commonly moss-like and complex, with spiky edges; embayments are often filled with palagonite and other alteration mineral assemblages. Bubble wall-like particle margins were rarely recognized and were restricted to the coarser ash fractions. In general, juvenile particles displayed low vesicularity with average bubble sizes in the range of tens of microns. Fine-ash glassy pyroclasts were typically altered. Glass particles smaller than 100 microns were difficult to distinguish. Therefore, total volume estimates for the potential interactive particles were not possible, and should be addressed in future research.

8. BSE Study

Backscattered electron microscopy (BSE) was employed to determine juvenile shape parameters and surface texture. The BSE images were taken at the Manawatu Microscopy Centre at Massey University on an FEI Quanta 200 (Eindhoven, The Netherland) operated under 20 kV acceleration with a dual backscattered electron detector.

Representative samples were taken and polished thin sections were prepared and carbon-coated for BSE imagery. The BSE imagery revealed that the juvenile particles are glassy and fractured, even in the few tens of microns particle-size ranges. The fine-fracture network identified in LM was enhanced using BSE imagery (Figure 7A,B). Larger particles (coarse ash) showed moderate vesicularity similar to that recognized in the LM study (Figure 7C). However, enhanced contrast of the BSE images revealed the smooth bubble walls of the vesicles (Figure 7D). The particle margins in both fine and coarse pyroclasts showed fractured, commonly moss-like, complex boundaries (Figure 7B,E). On BSE images, the boundary textures were easy to characterise and the images were ideal, in most cases, for image analysis. The BSE images elucidated the moss-like edges of coarse-ash particles, an attribute considered to be one of the main textural features common to the glassy pyroclasts in most of the samples reviewed, especially those derived from maar-diatremes developed over thick Neogene sedimentary successions.

The overall appearance of the glassy juvenile particles in each grain-size range was blocky with sharp edges (Figure 7F). Step-like margins, as well as zones of convoluted bulbous margins of coarse ash, were apparent in most cases (Figure 8A). The fine-ash fraction of the glassy pyroclasts was characteristically blocky, with large and sharp edges (Figures 7F, 8B).

The BSE images were especially useful when identifying the microlite content (Figure 8C,D), vesicle patterns (Figure 8E,F), and hidden fracture networks in the interior of the juvenile pyroclasts. Overall the BSE images illustrated that the glassy pyroclasts had a more characteristic blocky and edgy texture. The glassy pyroclasts showed many hidden fractures and a fractured outer margin, a feature which was not as strongly pronounced on LM images (Figure 7A). The fine-grained glassy pyroclasts were generally low in microlite content (Figure 8D), but occasionally larger olivine and pyroxene micro-phenocrysts were

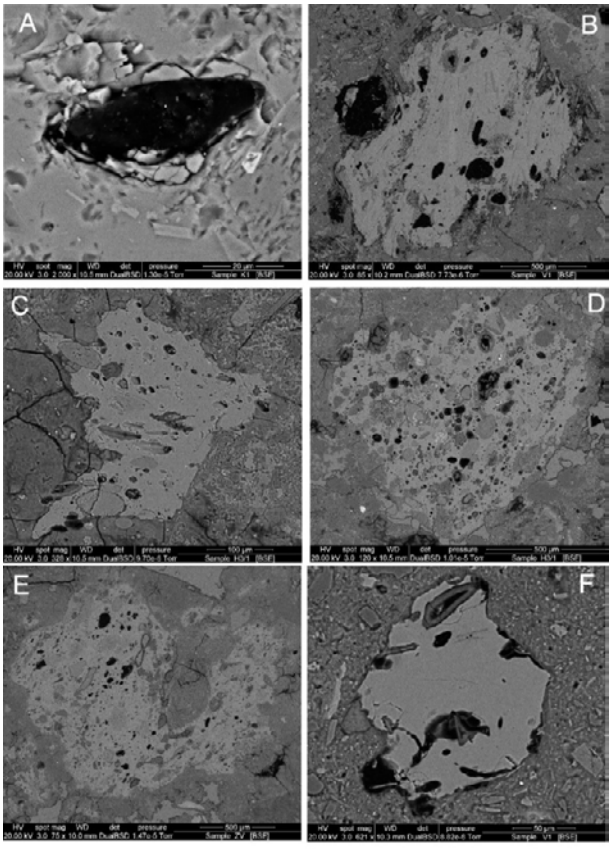

Figure 7. BSE images of volcanic glass shards included in the shape and fractal dimension studies. Note the micro fracture network (A – Kereki-domb diatreme) identified in a small-scale in nearly each of the analysed glass particle. The glass shards showed generally low vesicularity (B – Vendek-hegy diatreme; C – Hármas-hegy diatreme; D - Hármas-hegy diatreme), but moss-like sharp edges (E – Zánkai Vár-hegy diatreme). Active particles of fine ash were generally blocky and low in vesicularity (F – Véndek-hegy diatreme).

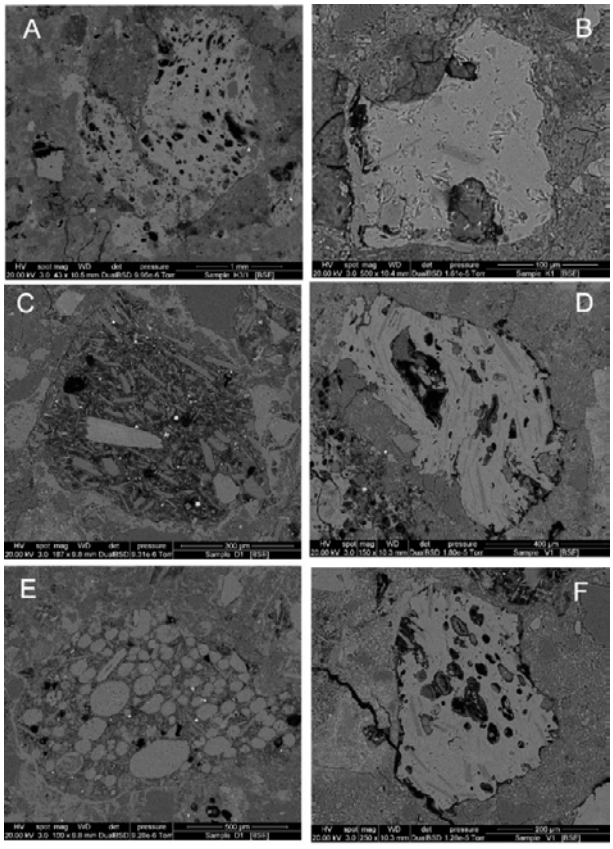

Figure 8. BSE images of volcanic glass shards included in the shape and fractal dimension studies. Note the common "fluidal" texture defined by microlite and stretched vesicles (A – Hármas-hegy diatreme). Fine ash particles were commonly flake-like, with sharp boundary with no vesicles or microlites (B – Kereki-domb diatreme). Microlite content variation was great, and especially coarser ash had high crystalinity (C – Kékkút diatreme). The microlites commonly defined fludal texture of the otherwise blocky pyroclasts of fine ash (D – Véndek-hegy diatreme). Vesicularity of the glass particles were generally low, but few foamy, basaltic reticulate-like clasts were also identified (E – Kékkút diatreme). The blocky shaped pyroclasts, even if they were fine grained, commonly showed distinct zones of vesicle-rich and microlite-rich zones (F – Véndek-hegy diatreme).

present and obscured the particle texture. Large olivine and pyroxene micro-phenocrysts were commonly formed in the marginal zones of pyroclasts. Their straight cleavage-determined boundary served in many cases as the glassy pyroclasts' margin. Such samples were disregarded in future image analysis, because the large boundary fraction of the minerals was more representative of the tendency for certain minerals to break in a particular pattern rather than the fragmentation style of the magma.

9. Volcanic Glass Shape Parameters

Morphological parameters of juvenile particles were measured and compared in order to characterize the mode of fragmentation of a particular particle and determine how it reached its present morphology. The concept of linking pyroclast-shape parameters to the potential processes that generated them is based on theoretical and experimental volcanological data. Magma fragmentation

during magma-water interaction is primarily caused by a molten fuel coolant interaction (MFCI) that produces two distinct groups of juvenile particles referred to as active (interactive) and non-active (passive or inactive) particles [2, 3, 5, 8]. Active particles are those that are directly involved in the thermal-to-mechanical energy transfer during the MFCI process, while non-active particles are fragments of the melt that are transported away from the fragmentation zone by the kinetic energy release of the MFCI [3, 71]. In other words, non-active particles are rapidly expelled when the melt is still liquid allowing for free air ductile fragmentation to occur, forming smooth surfaced particles [72]. Theoretically, active particles are smaller than 130 μm in diameter and are generated by brittle fragmentation; therefore, to "capture" the MFCI event, finer grain-size fractions need to be examined [2–5].

The ash fraction of selected phreatomagmatic rock samples derived from diatreme and proximal maar/tuff ring facies, ranging from about 300 microns to a few tens of microns in diameter, were examined to capture pyroclast textures and morphologies. This approach allows for the full range of fragmentation style, from purely brittle to purely ductile fashion, to be documented.

We used primarily BSE images during the analysis as high contrast greyscale images were relatively easy to transform to binary images (bitmap files) facilitating the application of segmentation and thresholding methods to capture the particle outlines. The contrast, especially between the background (commonly siliciclastic grains and mud rich matrix) and the selected glassy pyroclasts, was more pronounced in BSE images than in LM images, making it possible to obtain particle shape parameters from BSE images.

BSE images were transformed to black and white bitmap images and the *ImageJ* software package (http://rsbweb.nih.gov/ij/) was used to calculate standard shape parameters such as particle perimeter, particle surface area, and Feret diameter. Using these parameters we calculated the following dimensionless parameters as recommended by previous authors [3, 4, 9, 15, 16]: compactness (defined as the ratio of the particle area to the particle breadth multiplied by width, where the particle breadth is the distance between the leftmost and rightmost pixels of an object and the width is the distance between the uppermost and lowermost pixels of an object); elongation (defined as the ratio of the Feret diameter, the longest segment in an object, to the mean perpendicular intercept, the mean length of the chords of an object perpendicular to the Feret diameter); circularity (defined as the ratio of the particle perimeter to the perimeter of a circle with the same area of the particle); and rectangularity (defined by the ratio of the particle diameter to twice the sum of the particle breadth and width).

The input data in each data set were based on high quality black and white bitmap images. Semi-automated thresholding methods were used to separate particle outlines from background (matrix) instead of manual retracing of the particle outlines. Retracing a particle outline commonly misses vital micro-cracks, or fine micro-fractures in the margin, which are important in future discrimination studies to determine whether brittle or ductile deformation led to the particles' formation. Unfortunately, creating a black and white bitmap image that captures every fine detail of the particle is challenging due to the "uneven" original grey-scale images a real particle can produce on an image, due to sample quality, particle surface cover (e.g. alteration, adhering, or image quality problems in the interface between the particle and various holding media) (Figure 9A), or the level of interaction between the matrix and the particle (e.g. palagonitization, carbonate rim, oxidation) (Figure 9B).

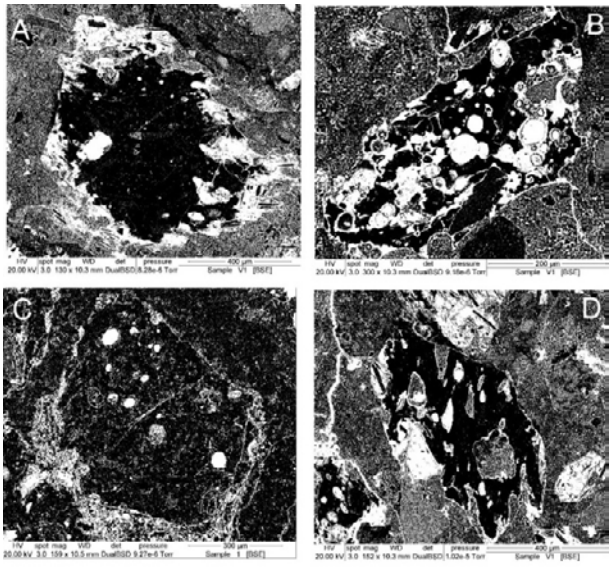

Figure 9. Image analysis of BSE images had some technical difficulty made the glass particle segmentation from the background complicated. Advanced palagonitization (A) commonly formed an "island-like" fresh glass interior (dark), and altered rim-like zone (light) made the segmentation impossible in automatically. Vesicle infill in glass particles also acted as difficulty in particle segmentation process (B). Fine grained carbonate rich matrix in few samples made the background very similar in grey-tone to the glass particle that obscured the exact segmentation of the particle from the background, and invoked manual retracing certain parts of the particle boundary (C). Elongated vesicles in few glass shards made the glass particle very complex due to the deep embayment an open vesicle may formed in the glass (D).

Despite these technical difficulties, BSE images revealed a hidden fracture network, suggesting that the larger particles (100–500 μm) underwent a complex fragmentation history. These images were enhanced on the captured particle outline binary images (Figure 10). Separation of the glassy particles from the heterogeneous siliciclastic background required some semi-automated thresholding. While thresholding was applied to separate the boundary of the glassy particles from the background, an interactive control with the original image was utilized, and if it was necessary, limited manual touch-ups were performed. Automatic thresholding was calculated by the *ImageJ* software based on the image's overall texture. Therefore, the particles, especially the complex ones, became fragmented and more "complex". To avoid creating artificial complexity, we also adjusted the threshold level manually. In addition, using pixel erosion (e.g. a certain layer of pixels "eroded" along any edges in the image) certain hidden sections of the fracture network became more pronounced, while an overall dilation of the image along the edges made the particle more homogeneous (e.g. the outline became more continuous) (Figure 10).

As an end-product, we followed the suggestion of Buttner et al. (2000) to plot a discrimination diagram of the circularity multiplied by the elongation values against the rectangularity multiplied by the compactness values (Figure 11). A clear trend is shown after plotting all the analyzed particle data on the same diagram: finer grained particles tend to plot on the brittle field of the diagram, suggesting a relationship between the active versus non-active particle shape parameters expected in fragmentation involved MFCI processes (Figure 11). The generated plots also show that those particle outlines obtained from automatic thresholding of the original images used to create the bitmap images plotted in the far end of the brittle fragmentation field, suggesting that the image analysis itself can create some complexity (Figure 11). This fact supports the method we used; however, we suggest that future studies using this method continually monitoring and evaluate the relationship between the generated and original image to maintain accuracy.

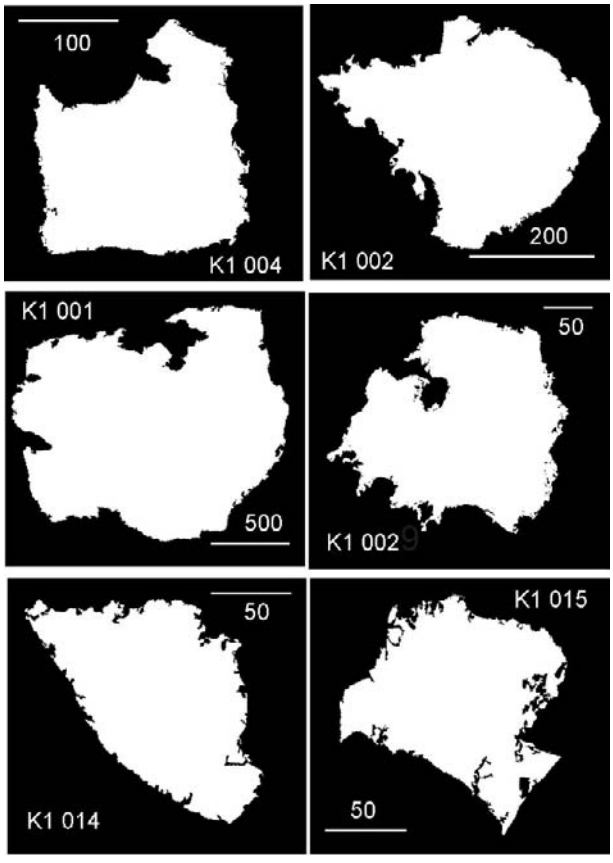

Figure 10. A series of particle outlines from the Kereki-domb diatreme pyroclastic rocks. Note the bulky and blocky appearance of the particles, but the complex boundary commonly fractured with peel-like zones.

10. Results of Particle-Shape Parameter Analysis

The particle-shape analysis suggests that BSE imagery is potentially more suitable for particle-shape analysis than light microscopy. Regardless of methodology, it is crucial to obtain an image that has not been artificially altered by adding extra complexity to the particle shapes during the creation of a bitmap image from full colour/greyscale natural samples.

The Buttner et al (2000) discrimination method is very sensitive to the particle boundary morphology, as such, accurate results depend on the usage of a high quality images (either grey scale or colour that can be transformed to black and white bitmap easily)e (Figure 11). In spite of the technical complications associated with obtaining high-quality shape parameters, the glassy juvenile particles from the phreatomagmatic lapilli tuff and tuff samples from the maar-diatreme volcanoes of Western Hungary demonstrate a clear trend. The larger (~200–300 μm) ash particles have shape parameters with a more ductile affinity (e.g. fall close to the boundary between the defined brittle to ductile fields), while the finer grained particles clearly plot in the brittle fragmentation fields of the Buttner et al. (2000) diagram (Figure 11). This trend indicates that rising magma underwent MFCI-triggered

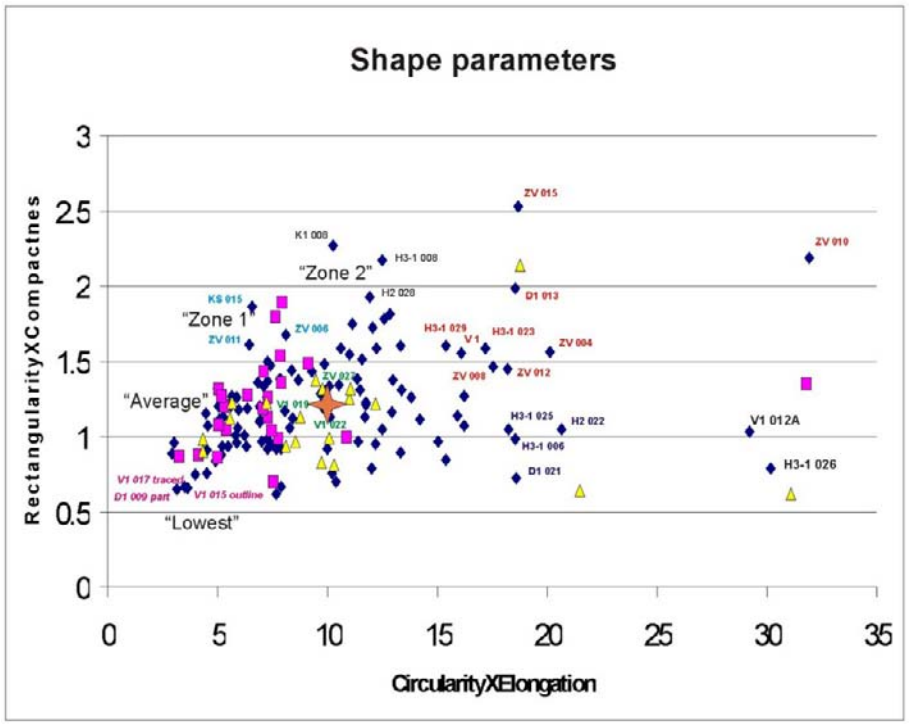

Figure 11. Shape discrimination diagram using Buttner et al 2002 method. According to Buttner et al 2002, "*rectangularity times compactness*" values over 1 are those that indicate brittle fragmentation (e.g. MFCI process) in the style of melt fragmentation. Note that the majority of the data plot near or above this value. The average value marked by an orange star. The lowest "*rectangularity times compactness*" values derived from those particles that were higher in vesicularity and size (coarse ash). Also samples that were manually retraced felt commonly below the discriminating value of 1. "Lowest", "Average", "Zone 1" and "Zone 2" refer to fields in the discrimination diagram from where the glass particle images were selected for visualisation in Figures 16, 17 and 18. Sample names correspond to the list provided in Figure 1.

explosive fragmentation and the generated kinetic energy dispersed larger, still fluid droplets of melt (coarse ash).

Data from two sites (Boglár and Kis-hegyestű diatreme) were plotted in separate discrimination diagrams to see if the potential shape parameter variations in individual samples differ between individual locations(Figure 12A,B). The data in both cases plotted in a very narrow field around the average dimensionless parameters for the whole population of Western Hungarian samples (Figure 12A,B), suggesting an overall similar fragmentation mode. The total distribution pattern of the total glass-shard-particle population showed a strongly skewed distribution of the "*circularity times elongation*" dimensionless parameter with a mean value of 9.93859 (Figure 13A). The "*rectangularity times compactness*" dimensionless parameter formed a more distinct distribution pattern with a mean value of 1.20611 and a skewness of 0.954296 (Figure 13B).

The presence of complex micro-fractures in the interior of the coarse-ash particles could be interpreted as a sign that they were derived from near the fragmentation front where the magma and water interacted. The complex particle morphology of the coarser ash fragments with fractured rims, moss-like boundaries, and relatively low vesicularity indicates that the melt underwent fragmentation and phreatomagmatic fragmentation as it was rising up the conduit. A phreatomagmatic fragmentation style is expected even in those sites where samples were dominated by coarse-ash to fine-lapilli-juvenile particles. Their overall glassy appearance, combined with the recognized micro-texture, suggests that in these locations magma was likely erupted in lava fountains through a wet environment. This scenario would explain the common fluidal texture defined by elongated micro-vesicles, and oriented microlites observed in the coarse-ash fractions in juvenile-rich pyroclastic rock samples.

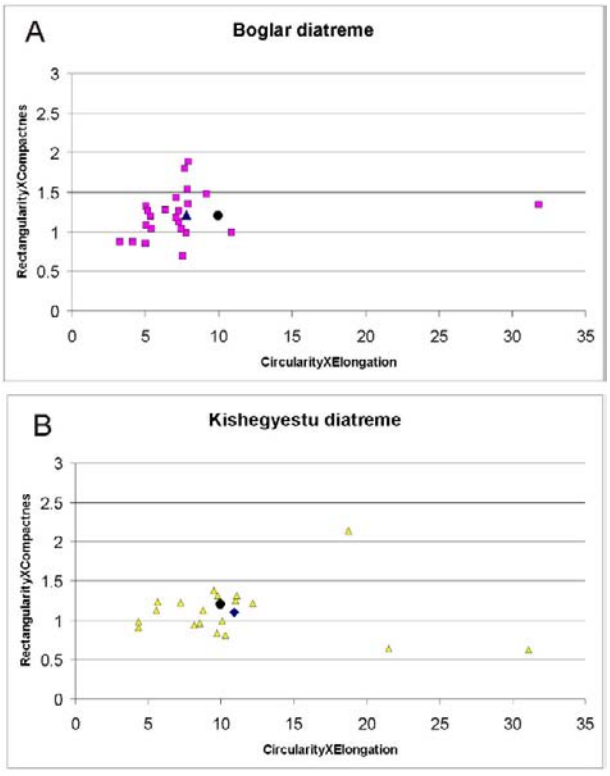

Figure 12. Shape discrimination diagrams using Buttner et al 2002 method with two individual locations; Boglár diatreme (A) and Kis-hegyestű diatreme (B). In both diagrams the entire field average value marked by a black filled circle. A black triangle represents the locality's average values on "A", while a black rectangle on "B".

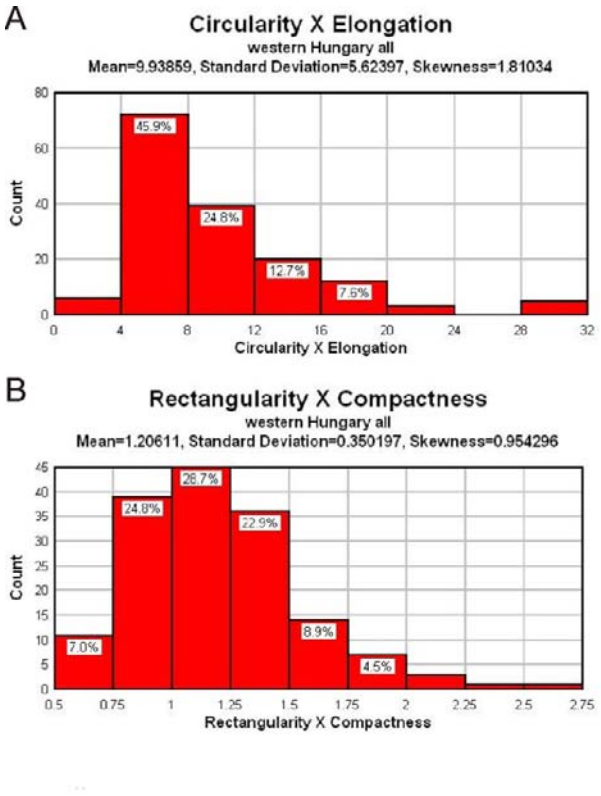

Figure 13. (A) "*Circularity times Elongation*" value distribution diagram from the entire data base.
(B) "*Rectangularity times Compactness*" value distribution diagram from the entire data base.

11. Fractal Dimensions of Glass Particles

A new technique implemented to characterize irregular particle boundaries, such as the boundary of volcanic ash, involves the use of fractal geometry and has been recently applied in various volcaniclastic sediments, both primary and reworked [15, 26, 73]. Fractal geometry, as related to particle morphology, is based on the concept that a convoluted space line, such as a particle boundary, can have a fractional dimension between 1 and 2, in contrast to the traditional Euclidean designation of 1 [74]. The term fractal is applied to an object whose morphological structure is the same, regardless of the scale at which it is viewed [74, 75]. Therefore, the fractal dimension can be viewed as a quantitative expression of the complexity of the particle boundary, in this case the ruggedness of an ash particle. While particle shape parameters and their dimensionless values, such as circularity, elongation, rectangularity and compactness [4], are proved to yield quantitative data that express the overall geometry of an ash particle, applying fractal dimension analyses to determine the complexity of ash particles can provide independent data that can be used to discriminate between certain complexities observed in ash particles. In this study we applied fractal analysis to calculate the general fractal dimension values of the volcanic glass shards from the phreatomagmatic rocks formed from maar-diatreme volcanoes in the Mio-Pleistocene monogenetic volcanic fields of Western Hungary.

In general, fractal dimension measurements of any particle (powder, aerosol, biological cell, sediment) primarily utilize two principal methods associated with length and mass [26, 76–78]. The two dimensional binary images generated from BSE imagery of polished petrologic thin sections naturally provide input data for applying fractal dimension calculations based on the length method. In this study, we provide an initial review of the fractal dimensions of the aforementioned ash particles.

Fractal dimensions were calculated using the "*calliper or ruler dimension method;*" a method based on the application of a series of linear step lengths of various sizes to approximate the total length of the particle perimeter [78]. As the step length (L) becomes smaller, the shape of an irregular boundary is more accurately reproduced. The relationship between the step length (L) and perimeter length (P) can be plotted as a line allowing the particle shape to be characterized. On a plot of log L versus log P (a so-called Richardson plot) [79], a straight line with a single slope represents a particle that has a self-similar, or true, fractal shape (i.e. morphological variations are the same at any scale). The fractal dimension (D) is related to the slope, S, of the log L versus log P plot by:

$$D = 1 - S \tag{1}$$

Values of D range from 1.0 to 2.0 with an increasing value corresponding to a more irregular boundary.

Many studies of natural particles have shown that Richardson plots based on length analysis do not typically yield curves with a single linear trend [15]. A common result is a data set that consists of at least two linear segments with different slopes [15]. These segments have been interpreted as a textural fractal related to small-scale irregularities on the particle surface and a structural fractal that describes the particle's macroscopic morphology [15, 24, 26, 73, 80]. Most natural particles have a textural fractal dimension that is less than the structural factor, reflecting the well-defined and relatively "smooth" particle boundary many particles have.

Particle boundaries that are characterized by two or more fractal dimensions are referred to as multifractal. While theoretically it appears straightforward to obtain fractal dimensions, creating a reliable and reproducible data set is challenging, as has been demonstrated in previous studies [73]. There are many difficulties associated with correctly selecting the textural and structural fractal values from a Richardson plot. To account for this, we primarily treated the generated lines as a single line without separating them into particle textural and structural fractal values. While this method certainly masked some details in the analysis, it still provided a data set that could be generated in a relatively fast and reliable way. Using the regression line of the log L versus log P diagram, we calculated the overall fractal dimension for each ash particle including both their textural and structural fractal dimension information. As a first order approach, the generated data set seemed to be valuable, easy to handle and reproducible. Particles were preferentially measured in the same image size in order to maintain a consistent size within and between samples so that the calculated fractal dimensions could be compared using *Benoit* commercial software (www.benoit.com).

12. Results of the Caliper Method

The perimeters of 157 ash particles were analyzed using the caliper method. The same data set was used to generate particle-shape parameters mentioned above. In general, the particles displayed the expected two fold (textural versus structural) linear segments in the Richardson plots. Interestingly, the regression analysis used to calculate the slopes and fractal dimensions, showed that the overall fractal dimension of each of the particles is similar to the particle textural fractal dimension values. This result validated our approach of using the overall fractal dimension values in our study.

The particles yielded an overall fractal dimension value that ranged between 1.50088 and 1.06802. The fractal dimension values for the entire data set formed a well distinguished unimodal distribution pattern with a mean fractal dimension value of 1.24521, a standard deviation of 0.0872938, and a skewness of 0.413891 (Figure 14). The skewed nature of the fractal dimension values indicates a well-centred, relatively low fractal-dimension value around 1.2 with a relatively broad tail of values scattered in a higher value fields.

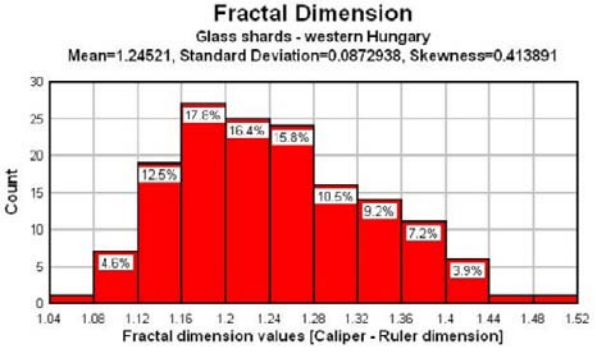

Figure 14. Fractal dimension distribution diagram of the studied glass particles using "*caliper*" or "*ruler*" fractal dimension calculations.

From a simplistic viewpoint, the higher the fractal dimension value the more complex the particle boundary. The average (1.237072876) fractal dimension values for the volcanic glass shards from phreatomagmatic pyroclastic rocks in Western Hungary (Figure 14) closely resembled the theoretical value of a Koch-flake (snowflake) that has a fractal dimension of log(4)/log(3) = 1.262.

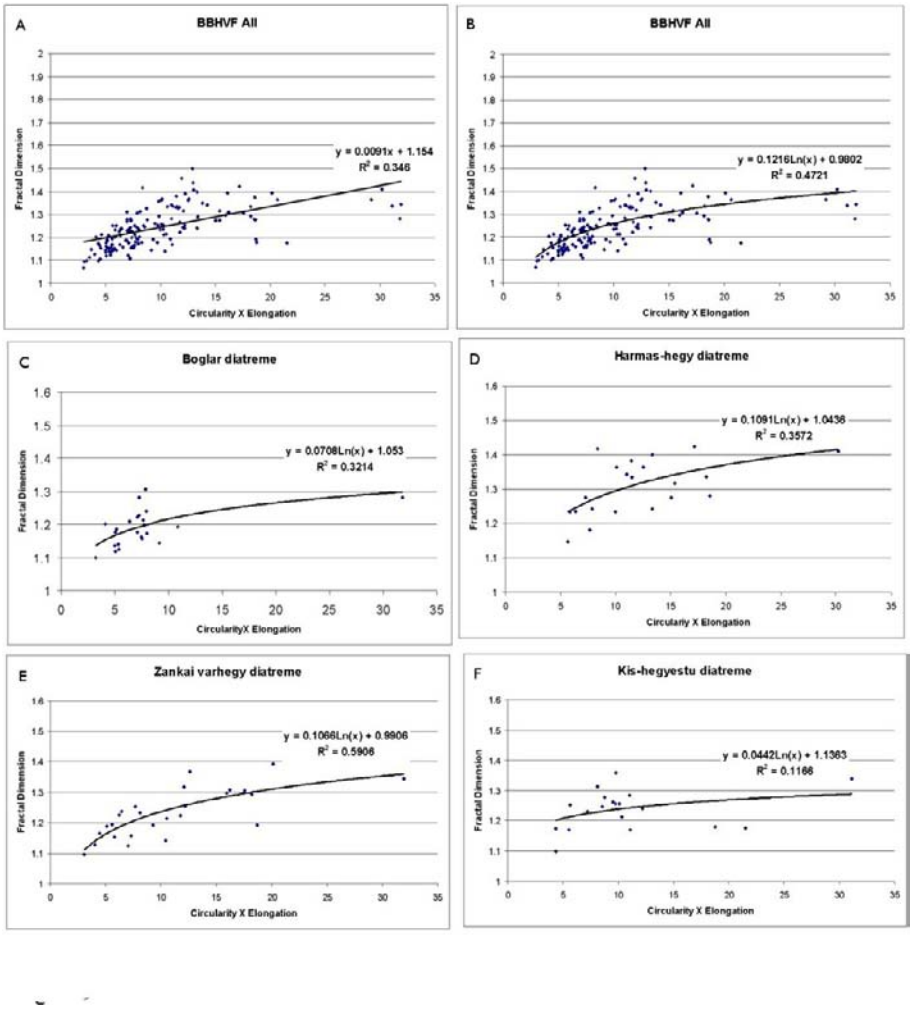

Figure 15. Fractal dimension values calculated for the all western Hungarian samples studied. On "A" a linear, while on "B" a logarhytmic regression line is fitted to identify trends.
On "C", "D", "E" and "F" fractal dimension values from an individual eruptive site are shown fitted with a logarhytmic regression lines. Note the similar trend in each diagram.

The fractal dimensions for volcanic glass particles produced by the caliper method suggest that the morphologies of the volcanic particles are "self-similar" at certain scales. Fractal dimension values appear to scatter over a well-centred, but large, field and can potentially be connected to certain particle shapes, a topic that can be explored in future research.

Fractal dimensions can be envisioned as a single numeric expression of the complexity of a particle boundary and can be connected with the dimensionless value of "*rectangularity times compactness*". In this respect, fractal dimension values are likely to be associated with certain particle shapes resulting from various deformation styles (e.g. ductile versus brittle). To test this concept, we plotted the "*circularity times elongation*" dimensionless values against the calculated fractal dimension values (Figure 15). The resulting data scatter plot (using the entire data base of glass shards from Western Hungary) showed a very characteristic distribution pattern that was best expressed by a logarhythmic trend rather than a linear trend line (Figure 15A,B). A remarkably similar data plot distribution occurs when the data plots from individual eruptive centres (Figure 15C,D,E,F) are separated, suggesting similar particle shape and fractal dimension parameters across the volcanic vent sites. The significance of this relationship and pattern cannot be understood yet and further research on more robust data sets is necessary.

13. Discussion

Certain fields of the particle shape discrimination diagram were examined closely, and the data points were compared to the visual manifestation of the glass particles. A series of cartoons have been created to visualise the dimensionless parameters and capture textural and shape features common to the glass shards from the phreatomagmatic successions (Figures 16, 17, 18). On Figure 16, a series of particles were selected to show the gradual textural changes among particles along the main trendline fitted on the overall data cloud on the discrimination diagram. The "*Lowest*" data group represents those particles that carry the least complex morphological features commonly associated with larger and higher vesicular glassy particles, inferred to represent those fragments that had the most ductile deformation in the course of the magma fragmentation (Figure 16). Particles assigned as "*Average*" are those representing particle shapes that fall along the average values calculated (Figure 16). In contrast, "*Zone 1*" and "*Zone 2*" are the most typical type of volcanic glass shard shapes from Western Hungarian phreatomagmatic eruptive centres (Figure 16), displaying features commonly thought to reflect a phreatomagmatic-fragmentation formation history [1, 9, 14, 81].

For comparison, the outlying glass shape types have also been illustrated on Figure 17 and Figure 18. These samples are those that show "extremely" high values and are commonly very complex with stretched shapes. Glass shards with high x and y values on the discrimination diagrams show similarities to moss-like complex pyroclasts formed by laboratory MFCI experiments (Figure 17). Strongly elongated glass types (Figure 18) are typically large (coarse ash), have a relatively high vesicularity, and likely represent melt fragments deformed in a ductile fashion prior to cooling.

While the particle shape parameter discrimination process applied in this work has powerful applications, usage of this method carries with it significant technical difficulties. Among these the most critical seems to be the particle segmentation technique using a heterogeneous sample. While SEM imagery of individual shards can be segregated from the homogeneous background with relatively little difficultly, BSE images can not be as easily manipulated. When the glass is hosted in fine-grained but complex mineral- and- rock-fragment assemblages such as matrix, it is especially important to continuously monitor the separation. The resulting bitmap images need to be visually validated and compared with the original samples. This is certainly time-consuming, but it seems to be the only way to obtain valuable results. In addition, the discrimination method is very sensitive to irregularities

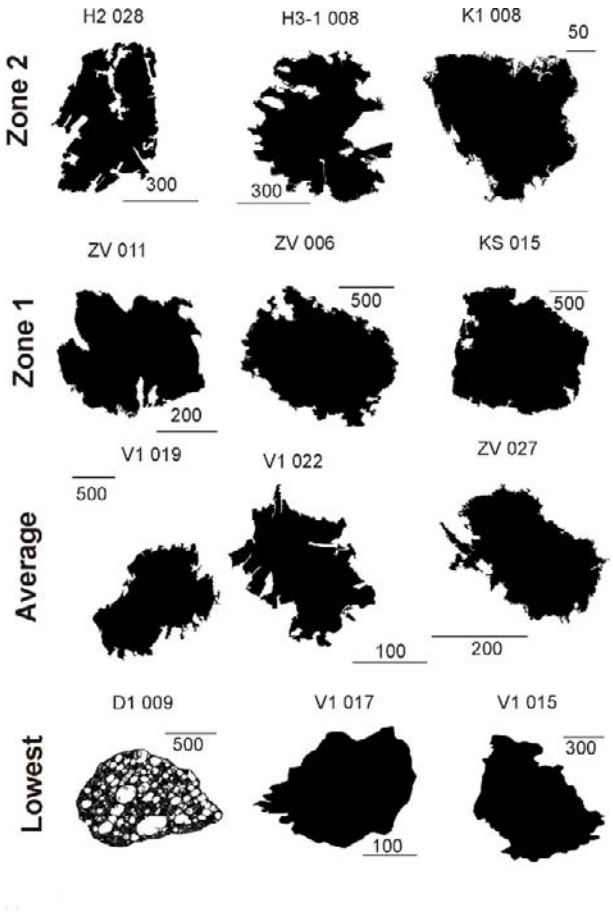

Figure 16. Visual representation of glass particles defining a gradual increase (from the lowest row to the top) of the "*rectangularity times compactness*" values. Scale bar values are in micron.

in the particle boundary on a few pixels scale, resulting in the loss of vital particle boundary information. On the other hand, using an automated segmentation method may create artificially complex particle boundaries through the use of poor thresholding methods. These difficulties can be overcome by integrating thin section studies with image analysis techniques, as presented in this paper. Overall, while some errors cannot be avoided, the discriminations still provide valuable data when characterizing the overall particle-shape parameters, especially if a large number of particles are involved in the analysis.

This study also encountered some significant problems dealing with particle boundary alteration features. Palagonitization and associated calcite precipitation and/or recrystallization of volcanic glass can, in particular, distort the original shape of the pyroclast. Such distortion can be overlooked, especially in BSE images, due to the fact that the newly formed alteration product can be very sim-

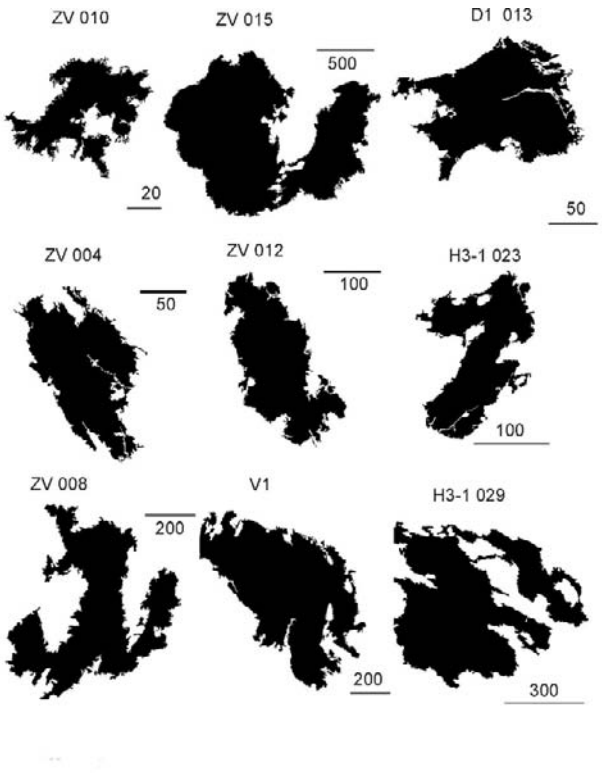

Figure 17. Visual representation of glass particles defining the highest "*rectangularity times compactness*" and "*circularity times elongation*" values. Scale bar values are in micron.

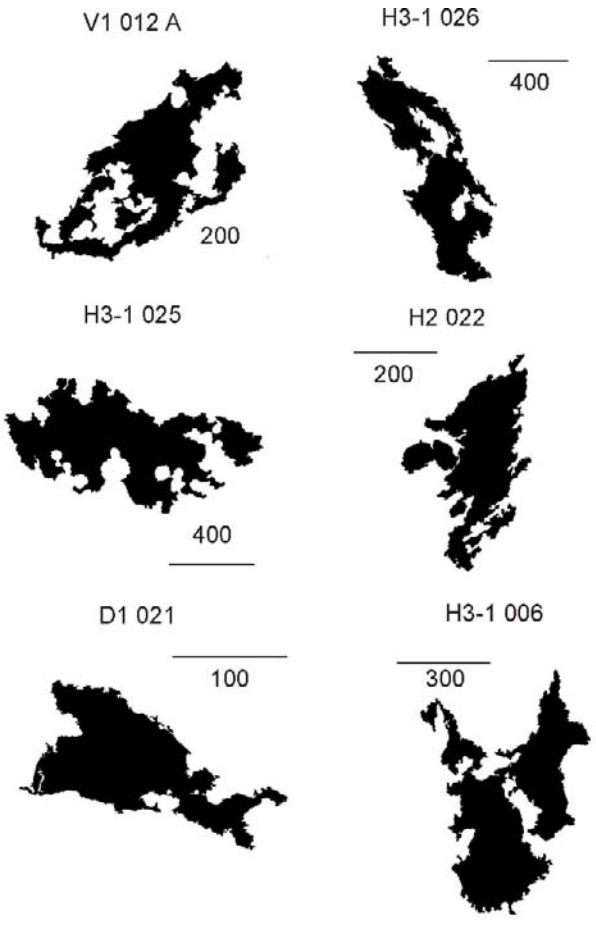

Figure 18. Visual representation of glass particles defining the highest "*circularity times elongation*" values.

ilar in texture and tone to the heterogeneous, commonly siliciclastic, fragment-rich matrix. In such cases, the measured and segmented glass could be nothing more than the still intact and preserved glass. Thus, the calculated shape parameters could reflect the alteration rather than the original fragmentation fashion. This issue also highlights the need for interactive sample processing, preferably by cross-checking various images with real samples to confirm or disregard such issues.

14. Conclusion

In this study we investigated the morphological characteristics of volcanic glass shards of maar-diatreme volcanic erosional remnants of the Mio-Pleistocene monogenetic volcanic fields of Western Hungary. The combined shape and fractal analysis revealed that the majority of the glass particles formed predominantly by brittle fragmentation, as expected from the results of the MFCI magma-and-water interaction. The majority of the volcanic glass shards are complex in shape, and closely resemble experimentally derived and natural phreatomagmatic glass shards from other phreatomagmatic volcanic fields. The complexity of glass shard shapes is seemingly scale-invariant, indicating that the fragmentation process that formed them acted in a similar fashion throughout the entire size spectrum. The best explanation of this is that not only was the fine ash formed by the MFCI processes, but the coarser fragments also went through a brittle-fashion fragmentation process. Such a scenario can be envisioned when hot magma shoots through a water-rich environment where fine ash forms at the interface between hot melt and external water and/or water-rich sediment, while coarse ash particles chilled rapidly, potentially "en-mass," prior to being dispersed by the released kinetic energy driven magma – water interaction. This study also highlighted the potential of shape and fractal analysis to be an effective methodology to employ when studying

older phreatomagmatic pyroclastic rocks. Analysis of such rocks can significantly contribute to our understanding of the processes that may have been involved during the formation of maar-diatreme volcanoes.

Acknowledgements

This paper was presented in the XIX Congress of the Carpathian Balkan Geological Association in Thessaloniki in 23-26 September 2010. To attend on the meeting was supported by the Massey University Leave & Ancillary Appointments Committee granted fund (LAAC10/37). BSE and SEM analysis was performed under the expert guidance of Doug Hopcroft at the Manawatu Microscopy and Imaging Centre in Palmerston North. The research was partially funded by and part of the research programs of the NZ IIOF, Massey University Research Fund and NZ FRST grants. Constructive comments by Journal reviewers and the Managing Editor, Katarzyna Cyran are greatly appreciated.

References

[1] Heiken G.H., Wohletz K.H., Volcanic Ash, University of California Press, Berkeley, 1986

[2] Zimanowski B., Wohletz K., Dellino P., Buttner R., The volcanic ash problem, J. Volcanol. Geoth. Res., 2003, 122, 1-5

[3] Buttner R., Dellino P., La Volpe L., Lorenz V., Zimanowski B., Thermohydraulic explosions in phreatomagmatic eruptions as evidenced by the comparison between pyroclasts and products from Molten Fuel Coolant Interaction experiments, J. Geophys. Res.-Sol. Ea., 2002, 107, 2277

[4] Buttner R., Dellino P., Zimanowski B., Identifying magma-water interaction from the surface features of ash particles, Nature, 1999, 401, 688-690

[5] Morrissey M.M., Zimanowski B., Wohletz K., Büttner R., Phreatomagmatic fragmentation. In: Sigurdsson H., Houghton B.F., McNutt S.R., Rymer H., Stix J., (Eds), Encyclopedia of Volcanoes, Academic Press, New York, 2000, 431-446

[6] Zimanowski B., Buttner R., Lorenz V., Hafele H.G., Fragmentation of basaltic melt in the course of explosive volcanism, J. Geophys. Res.-Sol. Ea., 1997, 102, 803-814

[7] Frohlich G., Zimanowski B., Lorenz V., Explosive thermal interactions between molten lava and water, Exp. Therm. Fluid Sci., 1993, 7, 319-332

[8] Buttner R., Dellino P., Raue H., Sonder I., Zimanowski B., Stress-induced brittle fragmentation of magmatic melts: Theory and experiments, J. Geophys. Res.-Sol. Ea., 2006, 111

[9] Dellino P., LaVolpe L., Image processing analysis in reconstructing fragmentation and transportation mechanisms of pyroclastic deposits. The case of Monte Pilato-Rocche Rosse eruptions, Lipari (Aeolian islands, Italy), J. Volcanol. Geoth. Res., 1996, 71, 13-29

[10] Heiken G.H., Wohletz K., Fragmentation processes in explosive volcanic eruptions. In: Fisher R.V., Smith G.A. (Eds.), Sedimentation in Volcanic Settings, Society for Sedimentary Geology, 1991, 19-26

[11] Wohletz K.H., Explosive magma-water interactions: Thermodynamics, explosion mechanisms, and field studies, B. Volcanol., 1986, 48, 245 - 264

[12] Wohletz K.H., McQueen R.G., Experimental studies in hydromagmatic volcanism. In: Studies in Geophysics: Explosive volcanism: Inception, evolution and hazards, National Academy Press, Washington, 1984, 158-169

[13] Wohletz K.H., Mechanisms of hydrovolcanic pyroclast formation - Grain-size, scanning electron-microscopy, and experimental studies, J. Volcanol. Geoth. Res.„ 1983, 17, 31-63

[14] Dellino P., Kyriakopoulos K., Phreatomagmatic ash from the ongoing eruption of Etna reaching the Greek island of Cefalonia, J. Volcanol. Geoth. Res.„ 2003, 126, 341-345

[15] Dellino P., Liotino G., The fractal and multifractal dimension of volcanic ash particles contour: a test study on the utility and volcanological relevance, J. Volcanol. Geoth. Res.„ 2002, 113, 1-18

[16] Dellino P., Isaia R., La Volpe L., Orsi G., Statistical analysis of textural data from complex pyroclastic sequences: implications for fragmentation processes of the Agnano-Monte Spina Tephra (4.1 ka), Phlegraean Fields, southern Italy, B. Volcanol., 2001, 63, 443-461

[17] Dellino P., La Volpe L., Structures and grain size distribution in surge deposits as a tool for modelling the dynamics of dilute pyroclastic density currents at La Fossa di Vulcano (Aeolian Islands, Italy), J. Volcanol. Geoth. Res., 2000, 96, 57-78

[18] Dellino P., Phreatomagmatic deposits: fragmentation, transportation and deposition mechanisms, Terra Nostra, 2000, 6, 99-105

[19] Lautze N.C., Houghton, B.F., Linking variable explosion style and magma textures during 2002 at Stromboli volcano, Italy, B. Volcanol., 2007, 69, 445-460

[20] Sable J.E., Houghton B.F., Del Carlo P., Coltelli M., Changing conditions of magma ascent and fragmentation during the Etna 122 BC basaltic Plinian eruption:

Evidence from clast microtextures, J. Volcanol. Geoth. Res., 2006, 158, 333-354
[21] Németh K., Monogenetic volcanic fields; their origin, sedimentary record, relationship with polygenetic volcanism, and how monogenetic they are. In: Canon-Tapia E., Szakacs A. (Eds.) What is a volcano? Geological Society of America, 2010 (in press)
[22] Kienle J., Kyle P.R., Self S., Motyka R.J., Lorenz V., Ukinrek Maars, Alaska .1. April 1977 Eruption Sequence, Petrology And Tectonic Setting, J. Volcanol. Geoth. Res., 1980, 7, 11-37
[23] Németh K., Cronin S.J., Charley D., Harrison M., Garae E., Exploding lakes in Vanuatu - "Surtseyan-style" eruptions witnessed on Ambae Island, Episodes, 2006, 29, 87-92
[24] Maria A., Carey S., Using fractal analysis to quantitatively characterize the shapes of volcanic particles, J. Geophys. Res.-Sol. Ea., 2002, 107, 2283
[25] Carey R.J., Houghton B.F., Sable J.E., Wilson C.J.N., Contrasting grain size and componentry in complex proximal deposits of the 1886 Tarawera basaltic Plinian eruption, B. Volcanolo., 2007, 69, 903-926
[26] Carey S., Maria A., Sigurdsson H., Use of fractal analysis for discrimination of particles from primary and reworked jokulhlaup deposits in SE Iceland, J. Volcanol. Geoth. Res.„ 2000, 104, 65-80
[27] Wada K., Fractal structure of heterogeneous ejecta from the Me-Akan Volcano, Eastern Hokkaido, Japan - Implications for mixing mechanism in a volcanic conduit, J. Volcanol. Geoth. Res., 1995, 66, 69-79
[28] Shea T., Houghton B.F., Gurioli L., Cashman K.V., Hammer J.E., Hobden B.J., Textural studies of vesicles in volcanic rocks: An integrated methodology, J. Volcanol. Geoth. Res., 2010, (in press)
[29] Dellino P., Lavolpe L., Fragmentation Versus Transportation Mechanisms in the Pyroclastic Sequence of Monte-Pilato Rocche-Rosse (Lipari, Italy), J. Volcanol. Geoth. Res.„ 1995, 64, 211-231
[30] Wohletz K., Krinsley D.H., Scanning electron microscopy of basaltic hydromagmatic ash, Scan. Electron Micros., 1978, 1-16
[31] Ersoy O., Aydar E., Gourgaud A., Bayhan H., Quantitative analysis on volcanic ash surfaces: Application of extended depth-of-field (focus) algorithm for light and scanning electron microscopy and 3D reconstruction, Micron, 2008, 39, 128-136
[32] Ersoy O., Gourgaud A., Aydar E., Chinga G., Thouret J.C., Quantitative scanning-electron microscope analysis of volcanic ash surfaces: Application to the 1982-1983 Galunggung eruption (Indonesia), Geol. Soc. Am. Bull., 2007, 119, 743-752
[33] Mangan M.T., Cashman K.V., The structure of basaltic scoria and reticulite and inferences for vesiculation, foam formation, and fragmentation in lava fountains, J. Volcanol. Geoth.. Res., 1996, 73, 1-18
[34] Mangan M.T., Cashman K.V., Newman, S., Vesiculation of basaltic magma during eruption, Geology, 1993, 21, 157-160
[35] Allen S.R., Bryner V.F., Smith, I.E.M., Ballance, P.F., Facies analysis of pyroclastic deposits within basaltic tuff-rings of the Auckland volcanic field, New Zealand, New Zeal. J. Geol. Geoph., 1996, 39, 309-327
[36] Von Veh M.W., Nemeth K., An assessment of the alignments of vents on geostatistical analysis in the Auckland Volcanic Field, New Zealand, Geomorphologie, 2009, 175-186
[37] Lorenz V., Kurszlaukis S., Root zone processes in the phreatomagmatic pipe emplacement model and consequences for the evolution of maar-diatreme volcanoes, J. Volcanol. Geoth. Res., 2007, 159, 4-32
[38] Lorenz V., Maar-diatreme volcanoes, their formation, and their setting in hard-rock or soft-rock environments, Geolines, 2003, 15, 72-83
[39] Németh K., Budai T., Diatremes cut through the Triassic carbonate platforms in the Dolomites? Evidences from and around the Latemar, northern Italy, Episodes, 2009, 32, 74-83
[40] Németh K., Martin U., Haller M.J., Alric V.L., Cenozoic diatreme field in Chubut (Argentina) as evidence of phreatomagmatic volcanism accompanied with extensive Patagonian plateau basalt volcanism? Episodes, 2007, 30, 217-223
[41] White J.D.L., Maar-diatreme phreatomagmatism at Hopi Buttes, Navajo Nation (Arizona), USA, B. Volcanol., 1991, 53, 239-258
[42] Lorenz V., Maars and diatremes of phreatomagmatic origin: a review, Transactions of the Geological Society of South Africa, 1985, 88, 459-470
[43] Martin U., Németh K., Mio/Pliocene phreatomagmatic volcanism in the western Pannonian Basin, Geologica Hungarica Series Geologica, Geological Institute of Hungary, Budapest, 2004
[44] Suhr P., Goth K., Lorenz V., Long lasting subsidence and deformation in and above maar-diatreme volcanoes - a never ending story, Zeitschrift der Deutschen Gesellschaft für Geowissenschaften, 2006, 157, 491-511
[45] Harangi S., Neogene magmatism in the Alpine-Pannonian Transition Zone - a model for melt generation in a complex geodynamic setting, Acta Vulcanologica, 2001, 13, 25-39
[46] Seghedi I., Downes H., Szakacs A., Mason P.R.D., Thirlwall M.F., Rosu E., Pecskay Z., Marton E., et al., Neogene-Quaternary magmatism and geodynam-

ics in the Carpathian-Pannonian region: a synthesis, Lithos, 2004, 72, 117-146
[47] Szabó C., Harangi S., Csontos L., Review of Neogene and Quaternary volcanism of the Carpathian Pannonian Region, Tectonophysics, 1992, 208, 243-256
[48] Cloetingh S., Lankreijer A., Lithospheric memory and stress field controls on polyphase deformation of the Pannonian basin-Carpathian system, Mar. Petrol. Geol., 2001, 18, 3-11
[49] Bada G., Horváth F., On the structure and tectonic evolution of the Pannonian basin and surrounding orogens. Acta Geologica Hungarica, 2001, 44, 301-327
[50] Horvath F., Royden L., The Pannonian Basin - a Study in Basin Evolution - Reply, Am. Assoc. Petr. Geol. B., 1990, 74, 1281-1282
[51] Bada G., Horvath F., Gerner P., Fejes I., Review of the present-day geodynamics of the Pannonian basin: progress and problems, J. Geodyn., 1999, 27, 501-527
[52] Bada G., Horvath F., Cloetingh S., Coblentz D.D., Toth T., Role of topography-induced gravitational stresses in basin inversion: The case study of the Pannonian basin, Tectonics, 2001, 20, 343-363
[53] Pécskay Z., Lexa J., Szakács A., Balogh K., Seghedi I., Konecny V., Kovács M., Márton E., et al., Space and time distribution of Neogene-Quaternary volcanism in the Carpatho-Pannonian region, Acta Vulcanologica, 1995, 7, 15-28
[54] Balogh K., Pécskay Z., K/Ar and Ar/Ar geochronological studies in the Pannonian-Carpathians-Dinarides (PANCARDI) region, Acta Geologica Academiae Scientiarum Hungaricae, 2001, 44, 281-301
[55] Szabó C., Falus G., Zajácz Z., Kovács I., Bali E., Composition and evolution of lithosphere beneath the Carpathian-Pannonian Region: a review, Tectonophysics, 2004, 393, 119-137
[56] Falus G., Szabó C., Vaselli O., Mantle upwelling within the Pannonian Basin: evidence from xenolith lithology and mineral chemistry, Terra Nova, 2000, 12, 295-302
[57] Németh K., Martin U., Large hydrovolcanic field in the Pannonian Basin: general characteristics of the Bakony- Balaton Highland Volcanic Field, Hungary, Acta Vulcanologica, 1999, 11, 271-282
[58] Balogh K., Németh K., Evidence for the neogene small-volume intracontinental volcanism in western Hungary: K/Ar geochronology of the Tihany Maar volcanic complex, Geologica Carpathica, 2005, 56, 91-99
[59] Balogh K., Itaya T., Németh K., Martin U., Wijbrans J., Than N.X., Study of controversial K/Ar and 40Ar/39Ar ages of the Pliocene alkali basalt of Hegyestű, Balaton Highland, Hungary: a progress report. Mineralia Slovaca, 2005, 37, 298-301
[60] Wijbrans J., Németh K., Martin U., Balogh K., Ar-40/Ar-39 geochronology of Neogene phreatomagmatic volcanism in the western Pannonian Basin, Hungary, J. Volcanol. Geoth. Res., 2007, 164, 193-204
[61] Németh K., Martin U., Late Miocene paleogeomorphology of the Bakony-Balaton Highland Volcanic Field (Hungary) using physical volcanology data, Zeitschrift für Geomorphologie, 1999, 43, 417-438.
[62] Martin U., Németh K., Eruptive and depositional history of a Pliocene tuff ring that developed in a fluviolacustrine basin: Kissomlyó Volcano (Western Hungary), J. Volcanol. Geoth. Res., 2005, 147, 342-356
[63] Sacchi M., Horváth F., Magyari O., Role of unconformity-bounded units in the stratigraphy of the continental record; a case study from the late Miocene of the western Pannonian Basin, Hungary. In: Durand B., Jolivet L., Horváth F., Ranne M., (Eds.), The Mediterranean basins; Tertiary extension within the Alpine Orogen., Geological Society of London, London, 1999, 357-390
[64] Magyar I., Geary D.H., Muller P., Paleogeographic evolution of the Late Miocene Lake Pannon in Central Europe, Palaeogeogr. Palaeoec., 1999, 147, 151-167
[65] Auer A., Martin U., Németh K., The Fekete-hegy (Balaton Highland Hungary) "soft-substrate" and "hard-substrate" maar volcanoes in an aligned volcanic complex - Implications for vent geometry, subsurface stratigraphy and the palaeoenvironmental setting, J. Volcanol. Geoth. Res., 2007, 159, 225-245
[66] Németh K., Martin U., Harangi S., Miocene phreatomagmatic volcanism at Tihany (Pannonian Basin, Hungary), J. Volcanol. Geoth. Res., 2001, 111, 111-135
[67] Németh K., Martin U., Csillag G., Erosion rate calculation based on eroded monogenetic alkaline basaltic volcanoes of the Mio/Pliocene Bakony-Balaton Highland Volcanic Field, Hungary, Geolines, 2003, 15, 93-97
[68] Martin U., Németh K., Blocky versus fluidal peperite textures developed in volcanic conduits, vents and crater lakes of phreatomagmatic volcanoes in Mio/Pliocene volcanic fields of Western Hungary, J. Volcanol. Geoth. Res., 2007, 159, 164-178
[69] Németh K., Martin U., Csillag G., Lepusztult maar/diatrema szerkezetek a Bakony-Balaton Felvidék Vulkáni Területröl (Eroded maar/diatrema structures from the Bakony-Balaton Highland Volcanic Field), Annual Report of the Geological Institute of Hungary, 2003, 83-99, (in Hungarian)

[70] Petrelli M., Poli G., Perugini D., Peccerillo A., Petrograph: a New Software to Visualize, Model, and Present Geochemical Data in Igneous Petrology, Geochem. Geophys. Geosyst., 2005, 6 (Q07011), DOI 10.1029/2005GC000932.
[71] Buttner R., Zimanowski B., Mohrholz C.O., Kummel R., Analysis of thermohydraulic explosion energetics, J. Appl. Phys., 2005, 98, 043524
[72] Zimanowski B., Buttner R., Lorenz V., Premixing of magma and water in MFCI experiments, B. Volcanol., 1997, 58, 491-495
[73] Maria A., Carey S., Quantitative discrimination of magma fragmentation and pyroclastic transport processes using the fractal spectrum technique, J. Volcanol. Geoth. Res., 2007, 161, 234-246
[74] Mandelbrot B.B., How long is the coast of Britain? Statistical self-similarity and fractional dimensions, Science, 1967, 156, 636-638
[75] Mandelbrot B.B., Multifractal power law distributions: Negative and critical dimensions and other "anomalies," explained by a simple example, J. Stat. Phys., 2003, 110, 739-774
[76] Kindratenko V.V., VanEspen P.J.M., Treiger B.A., VanGrieken R.E., Characterisation of the shape of microparticles via fractal and Fourier analyses of scanning electron microscope images, Mikrochimica Acta, 13, 1996, 355-361
[77] Ouillon G., Sornette D., Unbiased multifractal analysis: Application to fault patterns, Geophys. Res. Lett., 1996, 23, 3409-3412
[78] Clark N., Three techniques for implementing digital fractal analysis of particle shapes, Powder Technology, 1986, 46, 132139
[79] Clark N.N., Maeder A.J., Reilly S., Data Scatter in Richardson Plots, Particle & Particle Systems Characterization, 1992, 9, 9-18
[80] Orford J.D., Whalley W.B., The use of the fractal dimension to quantify the morphology of irregular-shaped particles, Sedimentology, 1983, 30, 655-668
[81] Heiken G.H., An atlas of volcanic ash., Smithsonian Earth Science Contributions, Smithsonian Press, Washington, 1974, 12, 1-101